Computers in Biology and Medicine 188 (2025) 109875

Contents lists available at ScienceDirect

Computers in Biology and Medicine

journal homepage: www.elsevier.com/locate/compbiomed

Simulations of left atrial appendage inversion procedure: Patient-specific models with different appendage geometries

Roberta Scuoppo [a], Silvia Puleo [a], Giuseppe Sausa [b], Stefano Cannata [c], Giovanni Gentile [d], Julius M. Guccione [e], Ghassan S. Kassab [f], Caterina Gandolfo [c], Salvatore Pasta [a,b,*]

[a] Department of Engineering, University degli Studi di Palermo, Viale delle Scienze Ed.8, Palermo, Italy
[b] Department of Research, IRCCS ISMETT, Via Tricomi, 5, Palermo, Italy
[c] Department for the Treatment and Study of Cardiothoracic Diseases and Cardiothoracic Transplantation, IRCCS-ISMETT (Istituto Mediterraneo per i Trapianti e Terapie ad alta Specializzazione), Palermo, Italy
[d] Radiology Unit, Department of Diagnostic and Therapeutic Services, IRCCS ISMETT, Via Tricomi, 5, Palermo, Italy
[e] Department of Surgery, University of California San Francisco, San Francisco, CA, 94143, USA
[f] California Medical Innovations Institute, 11107 Roselle, San Diego, CA, 92121, USA

ARTICLE INFO

Keywords:
Left atrial appendage
Left atrial appendage inversion
Finite-element
Fluid-solid interaction analysis

ABSTRACT

Atrial fibrillation (AF) increases the risk of thromboembolic events due to clot formation in the left atrial appendage (LAA). Traditional methods to mitigate AF-related risk involve surgical or percutaneous exclusion of the LAA. Recently, left atrial appendage inversion (LAAI) has been proposed as a device-free, minimally invasive alternative for treating AF. This study uses computational modeling to understand the biomechanical implications of LAAI on four distinct LAA phenotypes: Chicken wing, cactus, windsock, and cauliflower. Structural inversion by finite-element analysis revealed significant changes in stress distribution, with the inverted apex experiencing positive stress surrounded by compressive stress fields peaking at nearly −4 MPa. The use of a stress-growth law predicted tissue resorption in the inverted apex, aligning with clinical and animal studies. Flow velocity and vorticity post-LAAI were estimated using one-way fluid-solid interaction (FSI) modeling. The cactus and cauliflower morphologies showed vorticity maxima of 3.9 1/s and 4.9 1/s, with most vorticity values concentrated around the Q1 quartile. Conversely, the windsock phenotype exhibited lower vorticity risks, indicating a reduced likelihood of thrombogenic events. These findings suggest that patient-specific simulations may improve the development and application of LAAI therapy to optimize clinical outcomes in patients with AF.

1. Introduction

Atrial fibrillation (AF) is the most prevalent cardiac arrhythmia encountered in clinical practice, with a reported incidence of 4.70 per 1000 person-years in multicenter studies [1]. The prevalence of AF varies significantly with age, affecting approximately 2 % of individuals under 65 years, 9 % of those over 65 years, and nearly 18 % of the elderly population over 85 years [2]. This condition is of particular clinical importance due to the association with a fivefold increased risk of stroke—an event that is the second leading cause of mortality and the primary contributor to disability among the elderly [3]. The management of AF places a considerable financial burden on healthcare systems, with annual expenditures reaching as high as $26 billion [4].

According to the European Society of Cardiology guidelines, stroke prevention in patients with AF is of utmost importance and is primarily managed through anticoagulant therapy for the majority of patients [5]. However, oral anticoagulants necessitate continuous monitoring and are linked with a considerable risk of bleeding, especially in elderly patients or those with comorbidities [6]. Consequently, the occlusion or exclusion of the left atrial appendage (LAA) is frequently employed as a therapeutic alternative for patients who have contraindications to long-term anticoagulation. This strategy is particularly advantageous, as the LAA is the predominant site of thrombus formation, which can cause life-threatening events [7]. Current techniques for LAA closure involve a range of devices and surgical methods designed to permanently occlude or exclude the appendage. Nevertheless, percutaneous approaches can

This article is part of a special issue entitled: Cardiovascular Digital Twins published in Computers in Biology and Medicine.

* Corresponding author. Department of Engineering, University of PalermoItaly.
E-mail address: salvatore.pasta@unipa.it (S. Pasta).

https://doi.org/10.1016/j.compbiomed.2025.109875
Received 22 September 2024; Received in revised form 22 December 2024; Accepted 4 February 2025
Available online 17 February 2025

be associated with complications such as device migration, incomplete closure, and the potential for thromboembolic events [8].

The inversion of the left atrial appendage into the left atrium offers a promising alternative to current device-based therapies by leveraging the heart's natural tissue response mechanisms to achieve occlusion without the necessity for permanent implants [9].

The left atrial appendage inversion (LAAI) procedure utilizes a suction-based catheter device to achieve partial inversion of the LAA. The catheter is advanced into the LAA, where a suction flute attaches to the distal endocardium, enabling inward retraction and inversion. An adhesive is subsequently applied through a needle-tip hypo-tube to stabilize the inverted configuration. Following adhesive curing, catheter removal leaves the LAA apex securely sealed. By inducing compressive stresses within the inverted tissue, the LAAI approach promotes gradual tissue resorption, ultimately resulting in occlusion over time. This approach not only mitigates the risks associated with permanent devices but also takes advantage of the heart's intrinsic capacity for tissue remodeling. Studying the biomechanical response of inverted LAA and reverse growth dynamics are paramount to understand how different LAA phenotypes respond to the inversion process and thus patient outcome.

For a comprehensive assessment of the outcomes associated with the LAAI procedure, this study employed patient-specific computational modeling to predict and analyze the intramural stress distribution and flow dynamics across four distinct LAA morphologies: Chicken wing, windsock, cactus, and cauliflower. Specifically, finite-element simulations estimated the stress field near the LAAI region. The resulting wall stress were used as input for a stress-growth law for estimating the resorption of biological tissue due to changes in the auricle homeostasis. Subsequently, fluid-solid interaction (FSI) analysis was conducted on the LAAI models to gain insights into the hemodynamic environment within the inverted LAA. This allowed estimations of flow velocity and vorticity, which are critical to evaluating the thrombogenic potential of each morphology.

2. Methods

2.1. Patient study group and segmentation

A retrospective analysis was conducted to identify four patients with AF, each exhibiting distinct left atrial appendage LAA morphologies: Chicken wing, windsock, cactus, and cauliflower types (Fig. 1B). For each patient, dynamic computed tomography (CT) images were processed using Mimics software (v.21, Materialize, Belgium) to reconstruct the geometry of the left atrium. The end-diastolic phase was used for the segmentation of LAAI geometry, as this was found to be optimal for reducing motion artifacts and improving the clarity of anatomical boundaries. This process involved semi-automatic thresholding of contrast-enhanced images, followed by manual editing and smoothing, as previously described [10]. The resulting LA geometries were then exported as STL files for further processing in Rhinoceros software (v.7, McNeel & Associates, USA). Specifically, the four inlets (pulmonary veins) and one outlet (mitral valve) were defined by performing cuts perpendicular to the vessel ostia and the mitral annulus. The centerline of each LAA was reconstructed and subsequently used to guide the direction of appendage inversion in the structural simulations.

2.2. FEM analysis of LAAI

Each anatomical component was meshed using ICEM meshing software (v2021, ANSYS Inc., USA) following a convergence analysis. The discretization error was maintained below 1 %, with the maximum principal stress used as the output parameter for comparing different grid sizes. Consequently, each patient-specific model was meshed with unstructured triangular shell elements, employing an element size of 1.2 mm for the atrium and 0.6 mm for the LAA region. The biomechanical behavior of the left atrial tissue wall was modeled as a hyperelastic material, characterized by a third-order Ogden strain energy function:

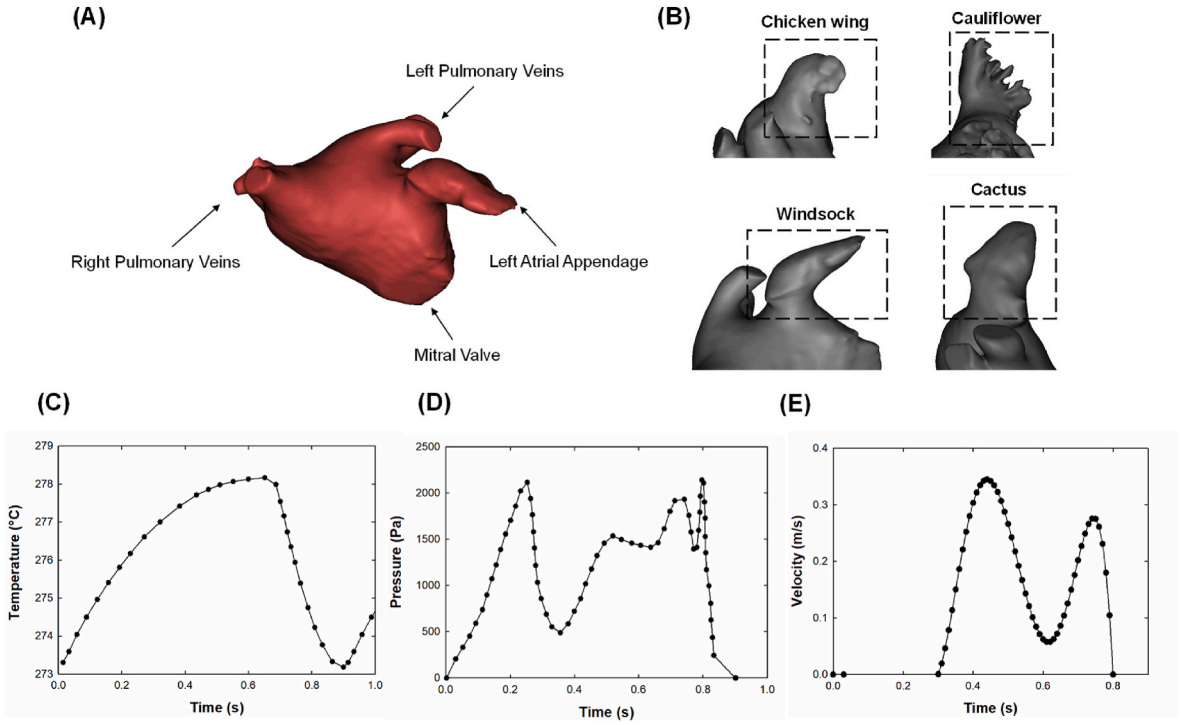

Fig. 1. (A) representative shape of left atrium with each appendage phenotype (B); (C) temperature profile for generating active contraction; (D) pressure waveform applied at each pulmonary vein as inflow condition; (E) flow velocity at mitral valve as outflow condition.

$$W = \sum_{i=1}^{3} \frac{\mu_i}{\alpha_i} (\lambda_1^{\alpha_i} + \lambda_2^{\alpha_i} + \lambda_3^{\alpha_i} - 3) \quad \text{Eq. 1}$$

where μ_i and α_i are material parameters and λ is the principal stretch. Specifically, the material parameters were: $\mu_1 = -56.13$ MPa, $\alpha_1 = 8.65$, $\mu_2 = 42.88$ MPa, $\alpha_2 = 10.03$, $\mu_3 = 13.59$ MPa, and $\alpha_3 = 6.82$ as obtained by biaxial testing of canine myocardium [11]. Incompressibility was enforced by setting the bulk moduli $D_i = 0, i = 1, 3$ in Ogden's constitutive model. A uniform thickness of 2 mm was adopted for the atrial wall and the material density was set to 1100 kg/m^3 according to literature data [12].

To simulate the LAAI procedure, the suction catheter clamping of the LAA was initially modeled by constraining the element nodes at the distal apex of the LAA. The subsequent inversion was simulated by pulling the clamped elements inward along the LAA centerline obtained during the segmentation process. The inversion process was implemented through connector assignments of the constrained nodes within the ABAQUS finite-element software (v2021hf7, Dassault Systèmes, USA). A velocity boundary condition was applied along the centerline direction to the central point of the connector, thereby mimicking the inversion of the distal portion of the LAA wall. The velocity magnitude was calibrated to replicate clinical observations, with a peak inversion speed of 10 mm/s, ensuring stable and realistic deformation dynamics.

To account for blood pressure during the inversion, a hydrostatic pressure of 1 mmHg was applied to the inner surface of the LA. The interaction of the LAA tissue wall with itself was considered using a general contact algorithm under frictionless conditions, with the explicit solver employed to address the nonlinearities and complex contact issues inherent in the simulation. Boundary conditions were applied to fix the distal ends of the pulmonary veins and the mitral valve in all directions. Energy monitoring was utilized to ensure a stable inversion, employing variable mass-scaling with a time step of 1x10^6 every 1000 iterations.

2.3. Reverse growth analysis

The central hypothesis considers that the partial inversion of the LAA will alter the stress distribution within the inverted appendage, disrupting homeostasis by reducing tensile ("positive") stress and potentially inducing compressive ("negative") stresses in the tissue wall. It is well-established that an increase in tensile stress can lead to tissue growth, whereas a decrease in stress may trigger tissue resorption, as described by a stress-growth law [13]. Given that the inverted state of the LAA alleviates stress, it is anticipated that the apex ("blind end") of the appendage may undergo resorption, ultimately eliminating the internal volume of LAA as part of the long-term tissue remodeling response following the LAAI procedure.

To elucidate the relationship between the deformation rate driven by reversible growth and the current stress state of the LAA material, a growth and remodeling equation is required. The model adopted in this study is grounded in the generic framework of volumetric strain-driven finite growth, utilizing a reversible growth multiplier (θ) within its formulation. The stress-growth modeling is achieved through the application of an isotropic growth tensor (F^g), which governs the growth dynamics in response to mechanical stimuli:

$$F^g = \theta \, \mathrm{I} \quad \text{Eq. 2a}$$

$$\frac{d\theta}{dt} = k(\theta)\phi(\lambda e) \quad \text{Eq. 2b}$$

where I is the identity tensor and λe is the elastic cardiac muscle stretch. In Eq. (2), the evolution of the growth multiplier depended on two scalar functions, namely, a rate limiting scalar function $k(\theta)$ and a growth driving function $\phi(\lambda e)$ that depends on the elastic stretch (λe). For reversible growth, the scalar function $k(\theta)$ and the growth driving function $\phi(\lambda e)$ assume the following functional forms when $\lambda e \leq \lambda_{h_1}$:

$$k(\theta) = \frac{1}{\tau_{rg}} \left(\frac{\theta - \theta_{min}}{\theta_{max} - \theta_{min}} \right)^{\gamma_{rg}} \quad \text{Eq. 3a}$$

$$\phi(\lambda e) = \lambda e - \lambda_{h_1} \quad \text{Eq. 3b}$$

where γ_{rg} is the degree of nonlinearity of sarcomere removal, τ_{rg} is a time-scale factor associated with reverse growth, θ_{max} and θ_{min} are the prescribed maximum and minimum values of the growth multiplier, λ_{h_1} is the homeostatic stretch value. The reversible growth of Eq. (3) aligns with the hypothesis that excessive stretch of the cardiac muscle beyond a certain homeostatic threshold (λ_{h_2}) induces growth, whereas reduced stretch below a different homeostatic threshold (λ_{h_1}) does not promote tissue growth. It is evident from Eq. (4) that growth terminates when either criterion $\theta = \theta_{max}$ or $\lambda e = \lambda_{h_2}$. On the basis that myocardial growth is reversible [13], then growth occurs in a way that the elastic stretch of the myocardial tissue is continually adjusted to remain within a homeostatic range $\lambda_{h_1} < \lambda e \leq \lambda_{h_2}$. To ensure that growth does not occur within the homeostatic range of the elastic stretch, we prescribed $\phi = 0$ when $\lambda_{h_1} < \lambda e \leq \lambda_{h_2}$. In this study, the growth parameters were assumed as $\tau_{rg} = 1$, $\gamma_{rg} = 1$ and $\lambda_{h_1} = 1.15$ as done by Lee et al. [13].

After simulation of LAAI procedure, tissue resorption was modeled using a pressure-time variation to simulate stretch-driven reverse growth. A cyclical low end-diastolic pressure of 2 mmHg over 10 cycles was applied successively to induce the reverse growth process. Each pressure cycle represents a time frame that may extend over several weeks rather than corresponding to a single heartbeat. The timescales of the cardiac cycle and reverse growth were calculated independently, with the growth multiplier updated only at the peak pressure of each cardiac cycle. While the cardiac cycle is defined by heart rate, the timescale for reverse growth was selected based on experimental data indicating the normalization of myocardial tissue characteristics over weeks to months [13]. This enabled the model to update the growth multiplier independently at the end of each cardiac cycle, without conflating the processes. The simulations of cyclical pressure were performed using the ABAQUS/Explicit solver, with post-processing done in Ensight software.

2.4. FSI analyses

Following the simulations of the LAAI procedure, one-way FSI analysis was performed by coupling ABAQUS with XFlow lattice-Boltzmann fluid dynamics software (v2022, Dassault Systèmes, USA) to estimate left atrial hemodynamics. The one-way FSI approach involved a unidirectional analysis in which the fluid solver received updated node positions and velocities from the structural simulation of the cardiac cycle. Specifically, the cardiac cycle was simulated by modeling the contraction of the left atrial myocardial wall using a thermal expansion analogy. The resulting deformation was transmitted to the flow solver at a time step of 0.001 seconds, with the LAA wall serving as the co-simulation interaction surface.

2.4.1. FEM analysis of cardiac cycle

In the structural solver, isotropic thermal expansion was combined with the Ogden material model for each inverted patient-specific model, following the methodology established by Musotto et al. [14]. The fictitious thermal expansion coefficient used to generate thermal stress was tuned through multiple simulations to achieve a 60 % difference between diastolic and systolic volumes, corresponding to the physiological ejection fraction of the LA. A virtual temperature profile was applied to simulate the time-varying active contraction of the left atrium (Fig. 1C), while a uniform pressure was applied to the luminal surface of the LA wall, in accordance with data from the literature [14].

To mitigate undesired high-frequency oscillations, a viscous pressure of 2.5×10^5 MPa was applied to the luminal surface of the left atrium for each appendage phenotype. As a boundary condition, the distal ends of

each outlet and inlet were fixed in all directions. The inverted portion was constrained to the appendage wall to replicate the tissue glue used during the LAAI procedure, ensuring the apex remained in the inverted state. A restart analysis was performed in ABAQUS to account for the stress field generated from the LAAI simulations. Two cardiac cycles, each with a duration of 0.9 seconds, were simulated for each FSI analysis.

2.4.2. Flow analysis

For the fluid solver, the deformed configuration of the LAAI was imported as the initial geometry for the FSI simulations. Blood was modeled as a Newtonian fluid, assumed to be isothermal at a temperature of 37 °C, with a dynamic viscosity of 0.0037 Pa s and a density of 1060 kg/m^3. Since the lattice-Boltzmann method is a meshless numerical technique where stability is governed by both temporal resolution and spatial discretization, preliminary fluid dynamics simulations were conducted to optimize the flow settings. The optimal ratio of spatial grid size to temporal resolution was determined to be dx/dt = 20, resulting in a temporal resolution of 2×10^{-4} s and a spatial resolution of 4 mm, with local refinement in the appendage region down to 0.2 mm.

Time-varying pressure waveforms were applied to the inlet pulmonary veins and a flow velocity outflow condition was imposed at the mitral valve (Fig. 1D and E). A no-slip boundary condition was enforced on the deforming left atrial wall. To ensure stable flow conditions within the LA, the distal ends of the pulmonary veins and the mitral valve were extended to eight times the diameter of each inlet and outlet. Two cardiac cycles were simulated, with the data from the final cycle used for post-processing.

3. Results

Deformed shapes resulting from the LAAI simulation procedures for each appendage phenotype were presented along with the corresponding stress distribution near the LAA wall (Fig. 2). The unique anatomical features of each appendage phenotype differentially influenced the outcomes of the LAAI simulations. The stress distribution at 50 % and 100 % completion of the LAAI procedure exhibited structural variations depending on the extent of inversion and the specific appendage morphology. At 50 % inversion, the stress distribution was primarily affected by the initial folding of the appendage apex, showing variations in stress values across different morphologies. At the end of inversion (i.e., 100 % LAAI), the folded apex generally displayed positive (tensile) stress, surrounded by a tissue wall exhibiting a negative (compressive) stress field. A 100 % inversion was defined as the complete folding of the LAA apex into the LA chamber, confirmed by the generation of compressive stress throughout the folded tissue. Although the magnitude of stress varied at the end of inversion, the overall stress pattern remained consistent across all LAAIs.

Profiles of maximum principal stress at the appendage apex as a function of simulation time were computed for each LAAI, as shown in Fig. 3. A steep decline in stress values was observed after the initial inversion steps, continuing until the conclusion of the LAAI simulation. The windsock-type LAAI exhibited a peak compressive stress of −3.9 MPa at 80 % of the inversion. In contrast, the cactus-type LAAI displayed a significant positive stress of 4.2 MPa at 65 % of the inversion, ultimately transitioning to a compressive stress field at the appendage apex at the end of the LAAI procedure as shown for other appendage morphologies.

Fig. 4 illustrates the evolution of LAAI anatomies color-coded with the reverse growth multiplier as predicted by the stress-resorption law. The magnitudes of the growth multiplier were evaluated at the end of the first, fifth, and tenth cycles of the idealized pressure experienced by the LAAI wall following inversion. The reverse growth process exhibited a peak multiplier value of 0.4 after the first pressure peak, initiating near

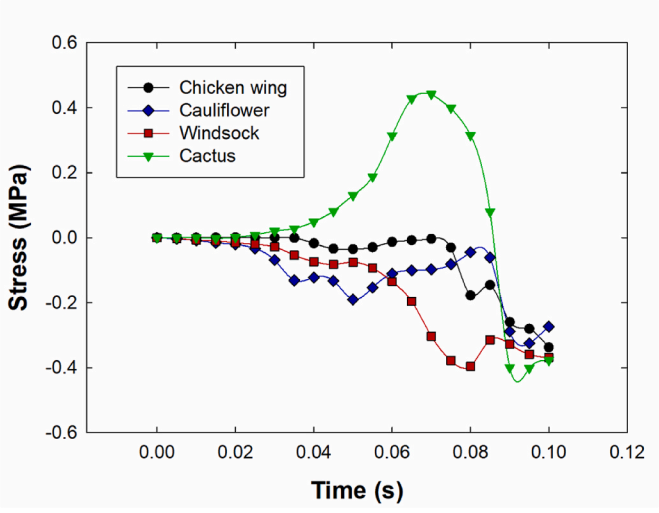

Fig. 3. Profiles of maximum principal stress at LAAI apex during simulation time for each appendage morphology.

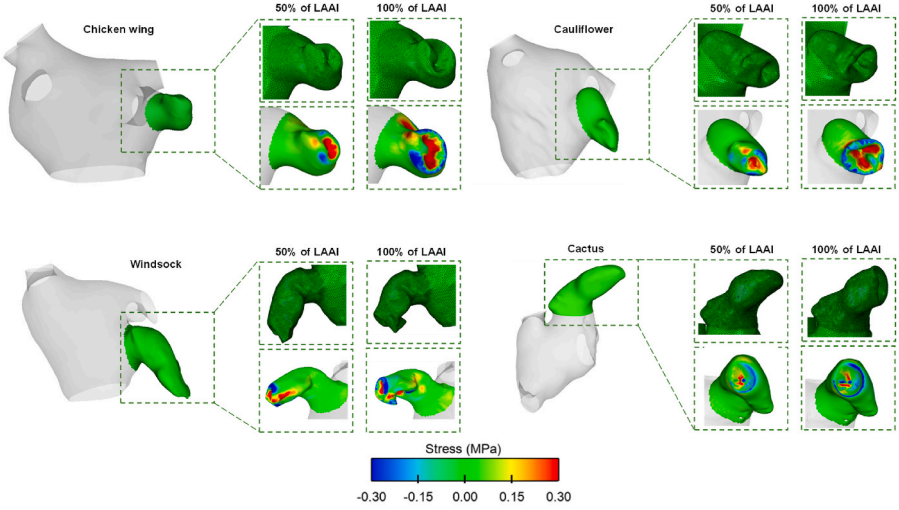

Fig. 2. Deformed LAAI and stress distribution for each appendage phenotype; the blue color highlights compressive stress around the apex wall while the red color indicates tensile stress regions.

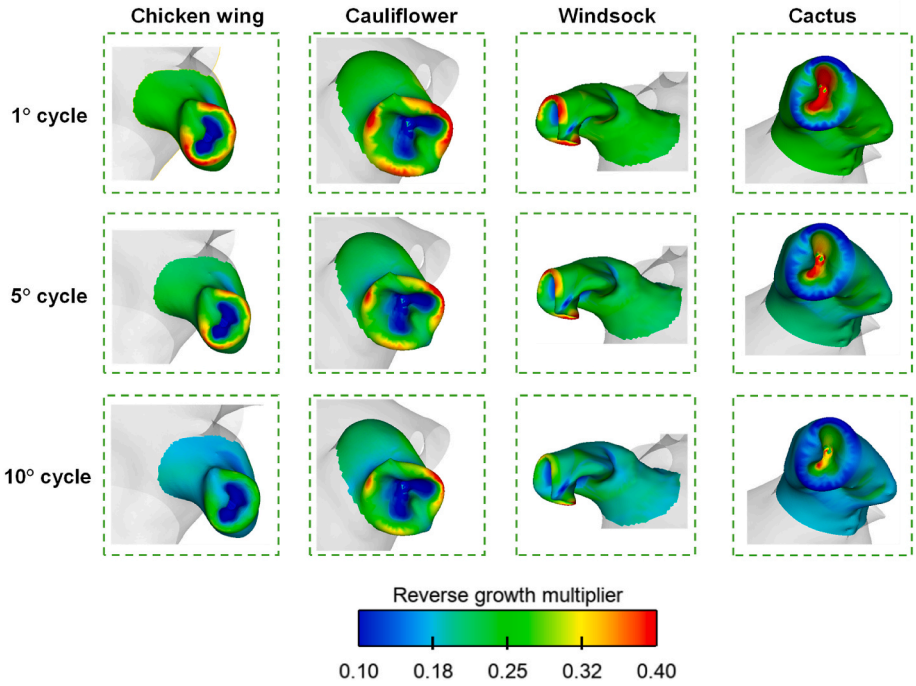

Fig. 4. Maps of tissue resorption as shown by the reverse growth multiplies for the LAA tissues. Trends of the reverse growth multiplier θ for each morphology: (A) Chicken Wing, (B) Windsock, (C) Cactus, and (D) Cauliflower. The graphs show how each morphology reaches a steady state during the reverse growth process.

the regions of negative pressure in the folded appendages. In contrast, growth values were lower in regions experiencing positive pressure and decreased with subsequent pressure cycles. The stress-mediated reverse growth stopped when the cardiac tissue stretch equaled the low homeostatic threshold.

Flow velocities from the FSI simulations of each LAAI were mapped onto the LA wall during both atrial systolic peak and diastolic phases, as shown in Fig. 5. Across all appendage types, flow velocities within the appendages were significantly lower than the flow magnitudes observed along the atrial wall throughout the cardiac cycle. No appreciable differences in the flow velocity were observed among the different appendage phenotypes. The velocity magnitude decreased progressively from the ostium of the LAA to the apex, indicating that the appendage apex is subject to fluid stasis, thereby increasing the risk of thrombosis.

Boxplots of time-averaged vorticity values over the cardiac cycle were computed for each LAAI morphology, with quartiles Q1, Q2, and Q3 fixed at 1.26, 2.27, and 3.54 1/s, respectively (see Fig. 6). This threshold of quartiles was computed by first performing the average of vorticity values for all LAAIs and then obtaining the quartiles. For the cactus morphology, vorticity peaked at 3.9 1/s, with the majority of vorticity values concentrated around Q1 as 49.45 % of the values fall within this range. The chicken wing morphology exhibited vorticity values ranging from 1.3 to 4.1 1/s, with most of the vorticity concentrated in Q3 and above. The windsock morphology displayed a broader

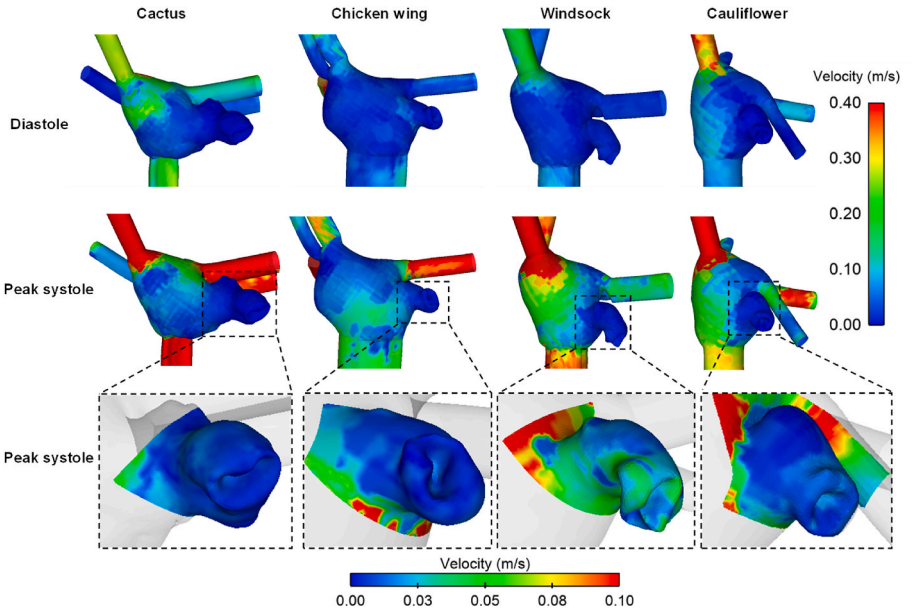

Fig. 5. Map of flow velocity at peak systole and diastole mapped on the left atrium wall for each appendage phenotype.

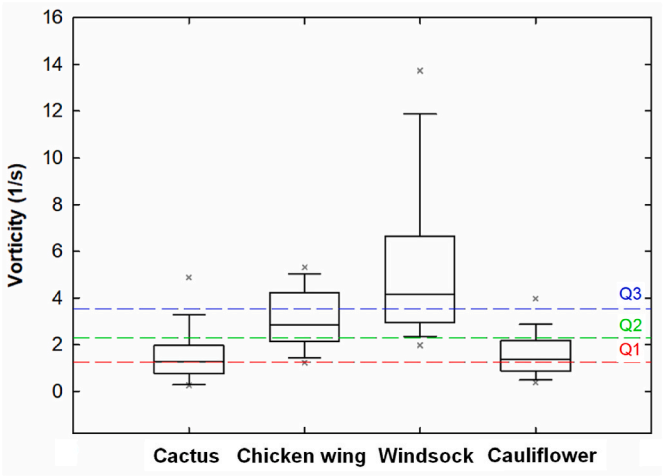

Fig. 6. Boxplot of vorticity values for each LAAI displaying the quartile values computed for the whole cardiac cycle.

variability in vorticity values, ranging from 2.3 to over 12.8 1/s, with a distribution heavily concentrated in Q3 and above. Lastly, the cauliflower morphology showed a maximum vorticity of 4.9 1/s, with the distribution primarily focused on Q1 and Q2, where nearly half of the values fell within Q1, and a significant portion was within Q2. Table 1 summarizes the percentage of vorticity values within each quartile range for the four LAAI morphologies.

Since several hemodynamic parameters, like vorticity, have been recognized by researchers as thrombosis predictor [15,16], maps of the vorticity parameter on the LAAI wall at both peak systole and diastole were computed and categorized into risk levels: low, mid, high, and critical, to identify regions with potential thrombosis risk (see Fig. 7). These risk thresholds were derived from the quartile values of the vorticity parameter for the four LAAI morphologies and were used to visualize areas of low and very low persistent vorticity, where blood flow may stagnate and increase the risk of clotting. The use of these risk thresholds allowed for a relative comparison of thrombogenic risk among morphologies, rather than an absolute prediction, providing a framework for evaluating potential high-risk regions.

During end-systole, the cactus morphology exhibited predominantly critical areas near the apex of the LAAI. In contrast, the chicken wing morphology showed high-risk regions throughout the cardiac cycle. The windsock morphology displayed primarily low to mid-risk areas over the cardiac cycle. The cauliflower morphology revealed pronounced critical vorticity areas, indicating significant flow vorticity in the LAAI wall. In diastole, the cactus morphology was the only phenotype to show a notable reduction in vorticity risk compared to the other LAAI phenotypes at the same phase of the cardiac cycle.

4. Discussion

This study was performed to quantify the biomechanical implications of the LAAI procedure to eliminate the LAA "dead" space and ultimately reduce the risk of clot formation associated with AF risk. This novel approach leverages mechanobiological stimuli to promote natural tissue resorption by altering the stress distribution (homeostasis) within the inverted region. We initially developed a structural finite-element model of the LAAI process and then quantified the tissue remodeling of inverted appendages over time using a stress-growth law. The biomechanical responses highlighted the distinct patterns of stress and reverse growth in the folded tissue across different appendage morphologies. Given the LAA's predisposition to a low-flow state, FSI analyses were performed to quantify vorticity and assess the thrombogenic potential for each appendage phenotype. Vorticity analysis revealed that the windsock morphology is most favorable to stable hemodynamics, thereby minimizing the risk of thrombus formation, while the cauliflower morphology posed significant hemodynamic challenges due to the irregular shape. For this reason, the LAAI procedure for the cauliflower phenotype suggests to invert each of the lobes to remove the apex by multiple inversion. While LAAI shows promise as a future clinical therapy for reducing clot formation, screening criteria should be established to assess the anatomical suitability of appendage morphologies to the inversion process. Such measures could enhance patient outcomes and reduce the risk of recurrent AF following the procedure.

Table 1
Percentage of time-averaged vorticity values within each quartile range for each LAA morphology.

	Q1 (%)	Q2 (%)	Q3 (%)	Q4 (%)
Cactus	49.95	32.97	9.89	7.69
Chicken wing	4.40	27.47	36.26	31.87
Windsock	0.01	8.79	36.26	54.95
Cauliflower	46.15	30.77	17.58	5.49

4.1. Stress analysis of inverted appendage phenotype

The change in the stress field due to the LAAI was previously described by our group using the high-fidelity left atrium geometry of the Living Heart Human Model [11]. We demonstrated the fundamental hypothesis that stress distribution shifts from tensile to compressive near the inverted appendage, and in this study, we extended the analysis across different LAA morphologies. Recently, Vella et al. [17] examined various LAA morphologies to assess how the apex shape responds to pressure changes during the inversion process. They found that the chicken wing morphology inverted at a lower pressure magnitude (−43 mmHg) compared to other morphologies (−88 mmHg for the cactus, −111 mmHg for the cauliflower, and −133 mmHg for the windsock), indicating a dependence of the inversion process on specific LAA morphology. Regarding stress, they reported a maximum principal stress of 3.5 MPa for the windsock appendage, which aligns with our stress predictions. In our study, the chicken wing and cauliflower models exhibited uniformly distributed compressive stress regions around the partially inverted apex, suggesting a favorable outcome for the inversion procedure in these morphologies. Conversely, the windsock model displayed a slight region of tensile stress, likely due to the presence of a belly along the longitudinal appendage direction, which hinders tissue folding.

It is important to note that our inversion process differs from the one simulated by Vella et al. [14]. Our study simulates the Kassab method, where a catheter device constrains and partially inverts the appendage apex, which is then held in place by tissue glue. In contrast, the Sternil method investigated by Vella et al. [17] involves hooking the inner tip with a catheter, using vacuum to draw the appendage into the left atrium, and then ligating it for final occlusion. Since our approach and that of Vella and collaborators aim to replicate different clinical procedures, differences exist in the stress patterns among the studies.

4.2. Reverse growth and tissue resorption

The adopted reverse growth model in our study calculated a growth multiplier based on principal stretch and demonstrated tissue resorption across all investigated LAA phenotypes. This finding is corroborated by echocardiography and histology performed on a normal swine four weeks post-LAAI procedure, as reported by our group [9]. The animal model showed the maintenance of the inverted auricle with evidence of cell resorption and an absence of thrombus or inflammation during the early follow-up period. This remodeling mechanism of the LAA is consistent with observations from epicardial exclusion procedures, where devices like the AtriClip and Lariat are used for epicardial clipping of the LAA ostia [18,19]. Although LAA remodeling has been

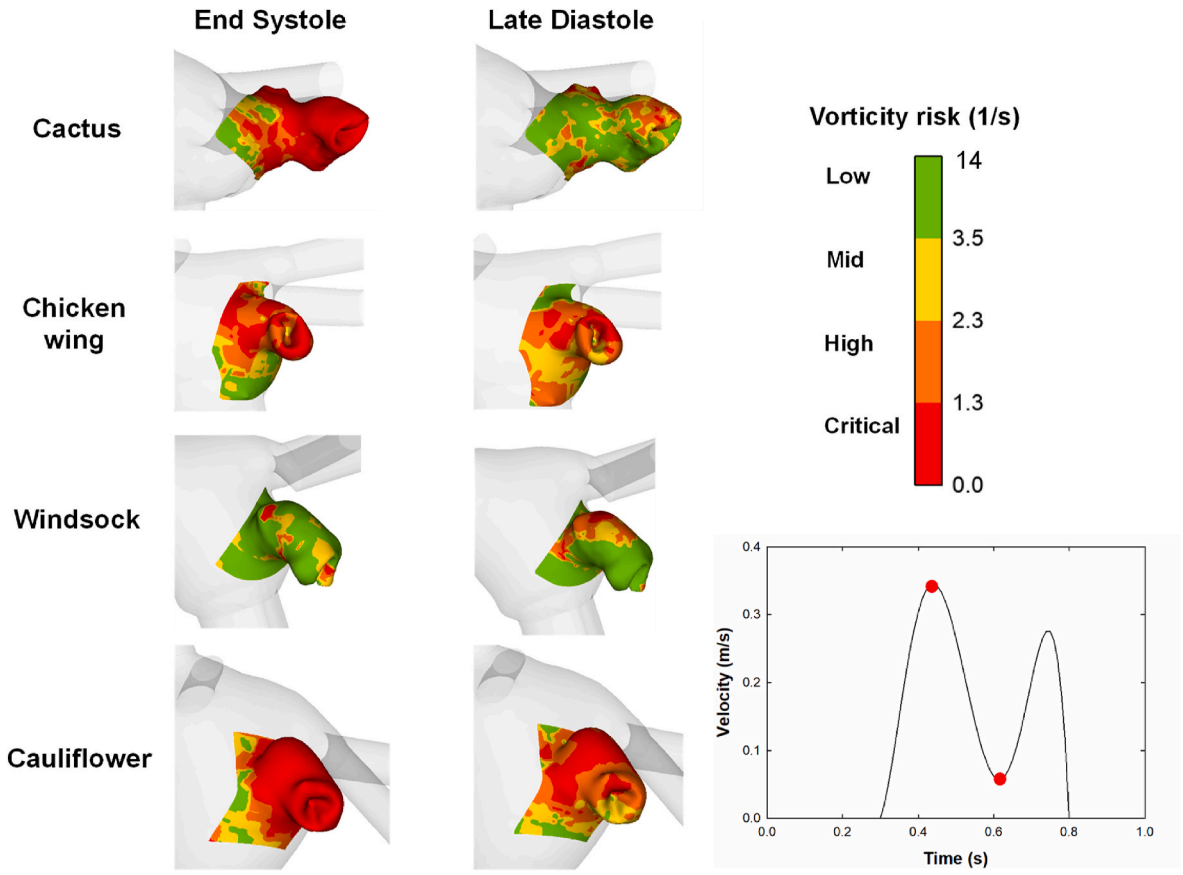

Fig. 7. Maps of the vorticity risk as indicator of the thrombogenic potential for each appendage morphology. Thrombogenic risk is highlighted by a four-leveled color bar graded from low, through mid, high and ending with critical thrombogenic risks.

clinically observed in patients following these procedures, the underlying pathophysiology of tissue resorption remains poorly understood.

We observed that all appendage phenotypes converged to a negative stress magnitude of nearly −4 MPa post LAAI. The shift from tensile to compressive stress appears to stimulate LAA remodeling by decreasing tissue mass due to reduced mechanical loading. This process is similar to the unloading effects observed in cardiac atrophy [20]. Indeed, hypertrophic growth of cardiomyocytes is a primary response by which the left ventricle reduces wall stress imposed by pressure overload, such as in hypertension. Conversely, cardiac atrophy is often observed in patients with heart failure who receive ventricular assist devices for prolonged periods, leading to an unloaded condition and subsequent tissue resorption.

Based on these considerations, the LAAI process may induce mechanobiological stimuli that promotes resorption and ultimately the elimination of the LAA apex. Chronic animal experiments are needed to support this hypothesis since atrial cardiomyocyte changes can happen within hours, while cardiac wall alterations usually take days, weeks, or even months. The growth parameters used in this study were adapted from prior experimental and computational research, ensuring alignment with observed tissue remodeling dynamics in preclinical models [12]. These parameters were chosen to replicate biologically relevant timescales and rates of tissue resorption. To evaluate the robustness of the conclusions, future studies will include sensitivity analyses to assess the impact of parameter variations on key outcomes, such as stress distribution and tissue resorption patterns.

4.3. Hemodynamic and thrombogenic potential

FSI analyses revealed significant variability in vorticity changes across different morphologies following the LAAI procedure. The windsock morphology emerged as the most favorable for achieving stable hemodynamics whilst the cauliflower morphology posed substantial flow differences due to its irregular shape. By using quartile values derived from the average vorticity estimates of all LAAIs, we were able to develop a vorticity risk map and perform a more detailed comparison of thrombogenic risks among different appendage morphologies. The windsock morphology exhibited the greatest variability in flow vorticity within the inverted appendage throughout the cardiac cycle, indicating smooth and consistent flow. Conversely, the cactus and cauliflower morphologies displayed a narrower range of vorticity predictions focused on the Q1, contributing to a likelihood of thrombosis.

In this context, computational flow analysis has been widely utilized to predict hemodynamic disturbances in the LAA and assess the risk of complications in both treated and untreated AF [14,21,22]. While most CFD studies in this topic typically use a rigid atrial wall [16,23], several investigations emphasize the importance of incorporating atrial motion. This can significantly affect the flow fields within the left atrial chamber. For instance, Corti et al. [24] demonstrated the value of including wall motion for a comprehensive stroke risk assessment, while Musotto et al. [21] highlighted FSI as an essential tool for accurately analyzing thromboembolic mechanisms in the LAA. However, no current studies in the literature specifically focused on the hemodynamic environment after auricle inversion. Wang et al. [9] performed in-vivo studies on the LAAI procedure. Their findings demonstrated that post-inversion, the morphology and histological staining revealed no significant inflammation or thrombus formation. Instead, tissue remodeling and fibrosis were observed at the inverted LAA site. Nevertheless, their study did not categorize or account for the potential influence of different LAA morphologies on the outcomes of the inversion procedure. Our FSI analysis aimed not to quantify the inherent risk for each patient post-inversion with the vorticity parameter but to elucidate the mechanisms

underlying adverse complications and explore their potential dependency on individual LAA morphology. By addressing this gap, our study provides insights into how the inversion procedure affects different LAA morphologies and their associated hemodynamic patterns.

5. Limitations

Several assumptions and simplifications were made in the computational modeling approach. The contractile action of the myocardium, the fiber-reinforced behavior of the left atrial wall, patient-variability in the LAA material properties, press-stress of left atrial wall and changes in appendage thickness were not considered. These factors could influence the deformed shape of the inverted appendage and alter the resulting stress field. Additionally, the stress-growth law used in the study did not account for changes in myocardial material properties or the evolving shape of the inverted appendage during reverse remodeling. Moreover, the growth parameters align with the resorption and sarcomere addition/removal rates observed in animal models [13] and may therefore differ from those in humans. Variations in mechanical properties could impact residual strain and, consequently, the prediction of tissue resorption over time. FSI analyses were limited to a one-way simulation, which did not capture the interactive dynamics typically present in bi-directional investigations. While the use of patient-specific LA and LAA geometries ensured realistic anatomies, the observed vorticity differences may reflect the combined influence of LAA and LA anatomies. Future studies with standardized LA models or larger patient cohorts could help isolate the specific effects of LAA morphology on post-inversion hemodynamics. Moreover, the level of thrombosis risk for each phenotype of LAA was evaluated using a quartile-based categorization to facilitate internal comparison across different morphologies. Future work should aim to develop standardized, clinically validated criteria for vorticity-based thrombosis risk assessment, incorporating both computational and experimental data to strengthen reliability. To simulate myocardial contraction, a thermal-analog model with isotropic assumptions was employed. Despite the presence of a transitional flow regime in the atrial chamber, the absence of a turbulence model may have led to an underestimation of changes in viscosity and affected flow vorticity predictions.

6. Conclusion

The LAAI procedure presents a promising, device-free alternative to current transcatheter and surgical therapies for stroke prevention in patients with AF. By partially inverting the LAA, the procedure eliminates the "dead" space within the auricle, reducing the potential for clot formation in this anatomical region. Patient-specific modeling of different LAA phenotypes was conducted to predict the structural and hemodynamic effects of the inversion procedure. The findings revealed significant variations in stress distribution, tissue remodeling, and flow vorticity among patients, suggesting a potential relation between appendage morphology and inversion outcomes that remains to be validated experimentally. These simulation results can guide the structural inversion of the LAA apex to optimize clinical management and outcomes following LAAI.

CRediT authorship contribution statement

Roberta Scuoppo: Writing – review & editing, Writing – original draft, Visualization, Software, Investigation. **Silvia Puleo:** Writing – review & editing, Writing – original draft, Software, Formal analysis. **Giuseppe Sausa:** Writing – review & editing, Writing – original draft, Software, Methodology. **Stefano Cannata:** Writing – review & editing, Writing – original draft, Data curation. **Giovanni Gentile:** Writing – review & editing, Writing – original draft, Data curation. **Julius M. Guccione:** Writing – review & editing, Writing – original draft, Conceptualization. **Ghassan S. Kassab:** Writing – review & editing, Writing – original draft, Conceptualization. **Caterina Gandolfo:** Writing – review & editing, Writing – original draft, Data curation. **Salvatore Pasta:** Writing – review & editing, Writing – original draft, Methodology, Data curation, Conceptualization.

Ethics approval and consent to participate

This study was approved by the IRCCS ISMETT Ethics Committee (approval no. IRRB04/04). All participants provided written informed consent prior to enrolment in the study.

Consent for publication

All authors were fully involved in the study and preparation of the manuscript which contribution originality can be confirmed by members of ISMETT and the University of Palermo. All authors approve the submission.

Availability of data and material

The datasets generated during and/or analysed during the current study are not publicly available due to ethical issues but are available from the corresponding author on reasonable request.

Ethics statement

All procedures were performed in compliance with relevant laws and institutional guidelines and have been approved by the appropriate institutional committee(s). Specifically, the study was approved by the IRCCS ISMETT Ethics Committee (approval no. IRRB04/04 – date April 2024). All participants provided written informed consent prior to enrolment in the study.

Funding

This project did not receive funding.

Declaration of competing interest

The authors declare that they have no known competing financial interests or personal relationships that could have appeared to influence the work reported in this paper.

References

[1] J. Kornej, et al., Epidemiology of atrial fibrillation in the 21st century: novel methods and new insights, Circ. Res. 127 (1) (2020) 4–20.
[2] C.T. January, et al., 2019 AHA/ACC/HRS focused update of the 2014 AHA/ACC/HRS guideline for the management of patients with atrial fibrillation: a report of the American college of Cardiology/American heart association task force on clinical practice guidelines and the heart rhythm society, J. Am. Coll. Cardiol. 74 (1) (2019) 104–132.
[3] A.S. Go, et al., Heart disease and stroke statistics–2014 update: a report from the American Heart Association, Circulation 129 (3) (2014) e28–e292.
[4] M.H. Kim, et al., Estimation of total incremental health care costs in patients with atrial fibrillation in the United States, Circ. Cardiovasc. Qual. Outcome. 4 (3) (2011) 313–320.
[5] G. Hindricks, et al., 2020 ESC Guidelines for the diagnosis and management of atrial fibrillation developed in collaboration with the European Association for Cardio-Thoracic Surgery (EACTS): the Task Force for the diagnosis and management of atrial fibrillation of the European Society of Cardiology (ESC) Developed with the special contribution of the European Heart Rhythm Association (EHRA) of the ESC, Eur. Heart J. 42 (5) (2021) 373–498.
[6] M. Molteni, C. Cimminiello, Warfarin and atrial fibrillation: from ideal to real the warfarin affaire, Thromb. J. 12 (1) (2014) 5.
[7] D. Lakkireddy, et al., Left atrial appendage closure and systemic homeostasis: the LAA HOMEOSTASIS study, J. Am. Coll. Cardiol. 71 (2) (2018) 135–144.
[8] D.R. Holmes Jr., et al., Left atrial appendage occlusion: opportunities and challenges, J. Am. Coll. Cardiol. 63 (4) (2014) 291–298.
[9] Y. Wang, et al., Safety and feasibility of left atrial appendage inversion in swine: a proof-of-concept study for potential therapy to prevent embolic stroke, Front. Bioeng. Biotechnol. 11 (2023) 1011121.

[10] F. Cosentino, et al., Statistical shape analysis of ascending thoracic aortic aneurysm: correlation between shape and biomechanical descriptors, J Pers Med 10 (2) (2020).
[11] S. Pasta, J.M. Guccione, G.S. Kassab, Inversion of left atrial appendage will cause compressive stresses in the tissue: simulation study of potential therapy, J Pers Med 12 (6) (2022).
[12] R. Karim, et al., Algorithms for left atrial wall segmentation and thickness - evaluation on an open-source CT and MRI image database, Med. Image Anal. 50 (2018) 36–53.
[13] L.C. Lee, et al., A computational model that predicts reverse growth in response to mechanical unloading, Biomech. Model. Mechanobiol. 14 (2) (2015) 217–229.
[14] G. Musotto, et al., The role of patient-specific morphological features of the left atrial appendage on the thromboembolic risk under atrial fibrillation, Front. Cardiovasc. Med. 9 (2022).
[15] A. Zingaro, et al., A comprehensive stroke risk assessment by combining atrial computational fluid dynamics simulations and functional patient data, Sci. Rep. 14 (1) (2024).
[16] A. Masci, et al., The impact of left atrium appendage morphology on stroke risk assessment in atrial fibrillation: a computational fluid dynamics study, Front. Physiol. 9 (2018) 1938.
[17] D. Vella, et al., Left atrial appendage inversion: first computational study to shed light on the phenomenon, Heliyon 10 (4) (2024) e26629.
[18] B. Kreidieh, et al., Left atrial appendage remodeling after Lariat left atrial appendage ligation, Circ. Arrhythm. Electrophysiol. 8 (6) (2015) 1351–1358.
[19] X. Liu, J. Pratt, J. Palmer, Successful fluoroless ablation of an incessant atypical atrial flutter attributed to AtriClip usage during mini-MAZE surgery for persistent atrial fibrillation, Heart. Rhythm. Case. Rep. 3 (7) (2017) 352–356.
[20] D. Burkhoff, S. Klotz, D.M. Mancini, LVAD-induced reverse remodeling: basic and clinical implications for myocardial recovery, J. Card. Fail. 12 (3) (2006) 227–239.
[21] G. Musotto, et al., Fluid-structure interaction analysis of the thromboembolic risk in the left atrial appendage under atrial fibrillation: effect of hemodynamics and morphological features, Comput. Methods. Progr. Biomed. 246 (2024) 108056.
[22] R. Koizumi, et al., Numerical analysis of hemodynamic changes in the left atrium due to atrial fibrillation, J. Biomech. 48 (3) (2015) 472–478.
[23] M. Garcia-Villalba, et al., Demonstration of patient-specific simulations to assess left atrial appendage thrombogenesis risk, Front. Physiol. 12 (2021) 596596.
[24] M. Corti, A. Zingaro, A.M. Quarteroni, Impact of atrial fibrillation on left atrium haemodynamics: a computational fluid dynamics study, Comput. Biol. Med. 150 (2022) 106143.